https://doi.org/10.5194/essd-2022-257
Preprint. Discussion started: 11 August 2022

Earth System Science Data
Open Access
Discussions

HiTIC-Monthly: A High Spatial Resolution (1 km×1 km) Monthly Human Thermal Index Collection over China from 2003 to 2020

Hui Zhang[1], Ming Luo[1,2*], Yongquan Zhao[3*], Lijie Lin[4], Erjia Ge[5], Yuanjian Yang[6], Guicai Ning[1,2], Jing Cong[7], Zhaoliang Zeng[8], Ke Gui[9], Jing Li[10], Ting On Chen[1], Xiang Li[1], Sijia Wu[1], Peng Wang[1], Xiaoyu Wang[1]

[1]School of Geography and Planning, Sun Yat-sen University, Guangzhou 510006, China.

[2]Institute of Environment, Energy and Sustainability, The Chinese University of Hong Kong, Hong Kong SAR, China.

[3]School of Geospatial Engineering and Science, Sun Yat-sen University, Zhuhai 519082, China.

[4]School of Management, Guangdong University of Technology, Guangzhou 510520, China.

[5]Dalla Lana School of Public Health, University of Toronto, Toronto, Ontario M5T 3M7, Canada.

[6]School of Atmospheric Physics, Nanjing University of Information Science & Technology, Nanjing 210044, China.

[7]Tianjin Municipal Meteorological Observatory, Tianjin 300074, China.

[8]State Key Laboratory of Severe Weather, Chinese Academy of Meteorological Sciences, Beijing 100081, China.

[9]State Key Laboratory of Severe Weather (LASW) and Key Laboratory of Atmospheric Chemistry (LAC), Chinese Academy of Meteorological Sciences, Beijing 100081, China.

[10]Collegee of Resources and Environment, Fujian Agriculture and Forest University, Fuzhou 35002, China.

**Correspondence to*: Ming Luo (luom38@mail.sysu.edu.cn) and Yongquan Zhao (yqzhao@link.cuhk.edu.hk)

https://doi.org/10.5194/essd-2022-257
Preprint. Discussion started: 11 August 2022

Open Access Earth System Science Data Discussions

Abstract

Human thermal comfort measures the combined effects of temperature, humidity, and wind speed, etc., and can be aggravated under the influences of global warming and local human activities. With the most rapid urbanization and the largest population, China is being severely threatened by aggravating human thermal stress. However, the variations of thermal stress in China at a fine scale have not been fully understood. This gap is mainly due to the lack of a high-resolution gridded dataset of human thermal indices. Here, we generate the first high spatial resolution (1 km×1 km) dataset of monthly human thermal index collection (HiTIC-Monthly) over China from 2003 to 2020. In this collection, 12 commonly used thermal indicators are generated by the LGBM machine learning algorithm from multi-source gridded data, including MODIS land surface temperature, topography, land cover and land use, population density, and impervious surface fraction. Their accuracies were comprehensively assessed based on observations at 2419 weather stations across the mainland of China. The results show that our dataset has desirable performance, with mean R^2, root mean square error, mean absolute error, and bias of 0.996, 0.693°C, 0.512°C, and 0.003°C, respectively, by averaging the 12 indicators. Moreover, the predictions exhibit high agreements with observations across spatial and temporal dimensions, demonstrating the broad applicability of our dataset. The comparison with two existing datasets also suggests that our high-resolution dataset can describe a more explicit spatial distribution of the thermal information, showing great potentials in fine-scale (e.g., intra-urban) study. Further investigation reveals that nearly all indicators exhibit increasing trends in most parts of China during the year 2003~2020. The increase is especially stronger in North China, Southwest China, the Tibetan Plateau, and parts of Northwest China, and in the spring and summer seasons. The HiTIC-Monthly dataset is publicly available via https://zenodo.org/record/6895533 (Zhang et al., 2022a).

https://doi.org/10.5194/essd-2022-257
Preprint. Discussion started: 11 August 2022

1 Introduction

Global climate change has brought significant challenges to human society and natural systems (Arias et al., 2021; Haines and Ebi, 2019), by inducing higher air temperature and more frequent extreme weather and climate events around the world (Arias et al., 2021; Schwingshackl et al., 2021). Heat-related disasters, e.g., heatwaves, droughts, and wildfires, are occurring more frequently and becoming more intense (Tong et al., 2021; Arias et al., 2021; Luo et al., 2022), exacerbating the thermal environment and threatening the tolerance limits of humans, animals, and plants (Raymond et al., 2020). Substantial warming and increasing extreme weather and climate events aggravate human thermal comfort and lead to increased exposures to uncomfortable thermal environments (Brimicombe et al., 2021), thus posing adverse impacts on public health, socio-economy development, and agricultural productivities (Budhathoki and Zander, 2019; Moda et al., 2019; Tuholske et al., 2021; Sun et al., 2019; Zhao et al., 2017).

The thermal stress that human beings actually perceive is not only related to air temperature, but also jointly influenced by other environmental variables such as humidity, wind, and/or direct sunlight (Mistry, 2020; Djongyang et al., 2010). These climatic variables alter the heat balance that maintains the core temperature of human bodies by influencing the heat exchange (e.g., radiation, convection, conduction, and evaporation) between humans and the surrounding environment (Periard et al., 2021; Stolwijk, 1975). High atmospheric humidity can exacerbate the thermal stress on human bodies by reducing evaporation from the skin through sweating when the air temperature is high (Li et al., 2018; Rogers et al., 2021; Luo and Lau, 2021). Furthermore, abnormal weather with a combination of extremely high air temperature, humidity, and/or wind can reduce labor capacity and human performance (Roghanchi and Kocsis, 2018; Lazaro and Momayez, 2020; Enander and Hygge, 1990), leading to temperature-related discomfort, stress, morbidity, and even death (Di Napoli et al., 2018; Kuchcik, 2021; Nastos and Matzarakis, 2011), particularly during heatwaves. For example, in the summer of 2017, 2018, and 2019, there were 1489, 1700, and 161 heatwave-related deaths, respectively, in the United Kingdom (Rustemeyer and Howells, 2021). Additionally, vulnerable groups, such as children, the elderly, chronic patients, and poor communities are at higher risk of being affected by thermal stress (Patz et al., 2005;

https://doi.org/10.5194/essd-2022-257
Preprint. Discussion started: 11 August 2022

Wang et al., 2019), which is likely to be further exacerbated as population aging and warming globally (United Nations, 2017).

The changes and impacts in human thermal stress have attracted increasing attention in recent years (Schwingshackl et al., 2021; Krzysztof et al., 2021; Li et al., 2018; Rahman et al., 2022; Ren et al., 2022; Luo and Lau, 2021). For instance, Szer et al. (2022) estimated the impact of heat stress on construction workers based on the universal thermal climate index (UTCI). Ren et al. (2022) and Luo and Lau (2021) explored the contribution of urbanization and climate change to the urban human thermal comfort in China. Schwingshackl et al. (2021) assessed the severity and trend of future global heat stress based on Coupled Model Intercomparison Project phase 6 (CMIP6). These studies were mainly based on meteorological stations or coarse-gridded data. However, the meteorological stations are sparsely distributed (Peng et al., 2019), particularly in undeveloped, mountainous, and oceanic areas, which cannot reveal continuously spatial distributions of air temperature and thermal stress conditions (He et al., 2021). Additionally, existing low spatial resolution image products (Mistry, 2020; Di Napoli et al., 2020) cannot be applied to fine-scale studies because they cannot provide information with spatial details and variations. However, the changes in human thermal stress at a fine scale (e.g., 1 km×1 km) remain much less understood. This research gap is mainly inhabited by the unavailability of a high spatial resolution (high-resolution) gridded dataset of human thermal stress.

Limited is high-resolution multiple human thermal stress indices dataset, compared with extensive studies in producing land surface temperature (LST) or near surface air temperatures (SAT). In particular, numerous LST datasets, such as Land Surface Temperature in China (LSTC) (Zhao et al., 2020) and the global seamless land surface temperature dataset (Zhang et al., 2022b; Hong et al., 2022), and near surface air temperature datasets such as ERA5 (ECMWF, 2017), TerraClimate (Abatzoglou et al., 2018), and GPRChinaTemp1km (He et al., 2021) have been produced. Few coarse-resolution human thermal stress datasets have been produced, such as ERA5-HEAT (Di Napoli et al., 2020), HDI_0p25_1970_2018 (hereafter, HDI) (Mistry, 2020), and HiTiSEA (Yan et al., 2021). ERA5-HEAT was derived from ERA5, which includes two global hourly human thermal stress indices (UTCI and mean radiant temperature (MRT)) from January 1979 to the present (Di Napoli et al., 2020) (Table S1).

https://doi.org/10.5194/essd-2022-257
Preprint. Discussion started: 11 August 2022

The HDI dataset was generated using 3-hourly climate variables of the global land data assimilation system (GLDAS), and it contains ten daily indices with a spatial resolution of 0.25°×0.25°, covering 90°N~60°S from 1970 to 2018 (Mistry, 2020). HiTiSEA contains ten daily human thermal stress indices from 1981 to 2017, with a spatial resolution of 0.1°×0.1° over South and East Asia (Yan et al., 2021), which was derived from ERA5-Land and ERA5 reanalysis products. However, these existing thermal index datasets have very coarse spatial resolutions. There is an urgent need for high-resolution (e.g., 1 km) dataset of human thermal stress.

Various indicators have been proposed to measure human thermal stress, and currently there is no universal or superior thermal stress indicator in all climate zones (Schwingshackl et al., 2021; Brake and Bates, 2002; Roghanchi and Kocsis, 2018; Luo and Lau, 2021). Existing human thermal stress indices have considered different climate conditions, direct or indirect exposures to weather elements, human metabolism, and the local working environment (Di Napoli et al., 2020). These indices have been designed to evaluate or quantify the comprehensive environmental pressure of temperature, humidity, wind, and other meteorological factors on human bodies (Epstein and Moran, 2006). They are based on the thermal exchange between the human and surrounding environments or empirical relationships gained by studying human responses to various environmental factors, varying in complexity, applicability, and capacity (Staiger et al., 2019). For example, the heat index (HI) is used for meteorological service (NWS, 2011); wet-bulb temperature (WBT) is used to measure the upper physiological limit of human beings (Raymond et al., 2020); physiologically equivalent temperature (PET) and UTCI are used to estimate human thermal comfort (Varentsov et al., 2020). A high-resolution dataset of different commonly used human thermal stress indicators is urgently called in global and regional studies, particularly for those with complex climate conditions (e.g., China).

China has been threatened by deteriorating thermal environments under global climate change and rapid local urbanization over the past decades (Ren et al., 2022; Luo and Lau, 2019). The changes and characteristics of human thermal stress across China have attracted extensive attention in recent years (Yan, 2013; Tian et al., 2022; Li et al., 2022). Wang et al. (2021) found that the frequency of extreme human-perceived temperature events increases in summer and decreases in winter in most urban

https://doi.org/10.5194/essd-2022-257
Preprint. Discussion started: 11 August 2022

agglomerations (UAs) of China. Li et al. (2022) found that the frequency of thermal discomfort days in China exhibits a significant increasing trend from 1961 to 2014, and there will be more threats from thermal discomfort in the future. Therefore, a long-term and high-resolution dataset with multiple human thermal stress indices in China is of great importance for studying detailed spatial and temporal variations of human thermal stress across the country. Such a dataset has the potential to (1) assess population exposure to extreme thermal conditions and heat-related health risks, (2) study the spatiotemporal evolution of human thermal stress and its influence on public health, tourism, industries, military, epidemiology, and biometeorology at a fine scale, and (3) provide the policymakers with data in manipulating targeted strategies to mitigate heat stress and protect vulnerable people.

In this study, we produced a high-resolution (1 km×1 km) thermal index collection at a monthly scale (HiTIC-Monthly) in China over a long period (2003 to 2020). This collection contains 12 widely used human thermal indices, including Surface Air Temperature (SAT), indoor Apparent Temperature (AT_{in}), outdoor shaded Apparent Temperature (AT_{out}), Discomfort Index (DI), Effective Temperature (ET), Heat Index (HI), Humidex (HMI), Modified Discomfort Index (MDI), Net Effective Temperature (NET), simplified Wet Bulb Globe Temperature (sWBGT), Wet-Bulb Temperature (WBT), and Wind Chill Temperature (WCT). The remainder of this paper is structured as follows. Sections 2 and 3 respectively introduce the data sources and describe the procedure for predicting the human thermal indices. Section 4 presents a comprehensive analysis of the accuracies and trends of the human thermal indices. Section 5 provides data availability. Section 6 compares our products with two existing datasets, and the main findings of this paper are summarized in Section 7.

2 Data

2.1 Meteorological dataset

Daily mean surface air temperature, relative humidity, and wind speed recorded at the 2419 weather stations across China (Figure 1) from 2003 to 2020 were collected from the China Meteorological Data Service Center (CMDC) at http://data.cma.cn/en. All station records were subjected to strict quality control and evaluation, including homogenization based on a statistical approach (Xu et al., 2013) and

https://doi.org/10.5194/essd-2022-257
Preprint. Discussion started: 11 August 2022

evaluation of temporal inhomogeneity based on the Easterling-Peterson method (Li et al., 2004).

2.2 Covariates

Human thermal stress is related to temperature, topography, land cover and land use, population density, surface water, and vegetation (Wang et al., 2020; Rahman et al., 2022; Krzysztof et al., 2021). In this study, eight variables reflecting the changes and spatial distribution characteristics of temperature were used to predict human thermal indices (Table 1) in addition to the meteorological variables. As LST is one of the most essential parameters for predicting human thermal indices, the seamless LST dataset created by Zhang et al. (2022b) was introduced into model training. This LST dataset used a spatiotemporal gap-filling algorithm to fill the missing or invalid value caused by clouds in the Moderate Resolution Imaging Spectroradiometer (MODIS) LST dataset (MOD11A1 and MYD11A1). It includes daily mid-daytime (13:30) and mid-nighttime (01:30) LST with 1 km×1 km spatial resolution. The mean root mean squared errors (*RMSEs*) of daytime and nighttime LST are 1.88°C and 1.33°C, respectively. The land cover and land use dataset developed by Sulla-Menashe and Friedl (2019) based on a supervised classification method was downloaded via Google Earth Engine (GEE). The Multi-Error-Removed Improved-Terrain (MERIT) elevation dataset developed by Yamazaki et al. (2017) was downloaded from GEE. This dataset was generated after removing the errors from existing Digital Elevation Models (DEMs), such as SRTM3 and AW3D-30m, based on multi-source satellite data and filtering algorithms. The spatial resolution of this dataset is 3″ (i.e., ~90 meters at the equator). In addition, the slope was also extracted from the elevation data to act as the topography predictor. As the artificial surface is closely related to human activities (Zhao and Zhu, 2022), the dataset of global artificial impervious area (GAIA) produced by Gong et al. (2020) from GEE was used to delineate human footprints. The overall accuracy of GAIA is greater than 90% (Gong et al., 2020). The population dataset was downloaded from the WorldPop Project (Gaughan et al., 2013). Then, the abovementioned eight datasets were pre-processed to have the same spatial extend, projection, and spatial resolution of 1 km×1 km through image mosaicking, reprojection, resampling, clipping, aggregating, and monthly synthesizing. Moreover, year and month of the year were also used as covariates.

https://doi.org/10.5194/essd-2022-257
Preprint. Discussion started: 11 August 2022

3 Methodology

3.1 Calculation of human thermal indices

In addition to SAT, the calculation of human thermal indices used in this study is described in Table 2. These indices are calculated based on SAT (also simply denoted as T), relative humidity (RH), wind speed (V), and actual vapor pressure (E_a). E_a is derived from T and RH, rather than directly observed at meteorological stations (Eqs. 1~2). Furthermore, monthly human thermal indices were derived by averaging daily values in each month.

$$E_s = 6.112 \times exp^{(17.67 \times T/(T+243.5))} \quad (1)$$

$$E_a = \frac{RH}{100} \times E_s \quad (2)$$

Here E_s is saturation vapor pressure (hPa) near the surface, T (℃) is air temperature at 2 m above the ground, and RH (%) is relative humidity at 2 m above the ground.

3.2 Prediction of human thermal indices using LGBM

The Light Gradient Boosting Machine (LGBM) algorithm was employed to predict human thermal indices from 2003 to 2020. Developed by Microsoft Research (Ke et al., 2017), LGBM is one of the gradient boosting decision tree (GBDT) algorithms. This algorithm has become a very popular nonlinear machine learning algorithm due to its superior performance in machine learning competitions and efficiency (Candido et al., 2021). Its performance has been evaluated and shows desirable results in different applications, such as evapotranspiration estimation (Fan et al., 2019), land cover classification (Candido et al., 2021; Mccarty et al., 2020), air quality prediction (Su, 2020; Zeng et al., 2021; Tian et al., 2021), subsurface temperature reconstruction (Su et al., 2021), and above-ground biomass estimation (Tamiminia et al., 2021).

LGBM adopts gradient-based one-side sampling (GOSS) and exclusive feature bundling (EFB) algorithms to improve the training speed (Su et al., 2021). GOSS is used to select data instances with larger gradients and to exclude a considerable proportion of small gradient data instances (Ke et al., 2017), and EFB is used to merge features (Ke et al., 2017). Compared with traditional GBDT algorithms including eXtreme gradient boosting (XGBoost) and stochastic gradient boosting (SGB), LGBM

https://doi.org/10.5194/essd-2022-257
Preprint. Discussion started: 11 August 2022

effectively decreases the training time without reducing the accuracy (Los et al., 2021; Ke et al., 2017). We used the Python package *Scikit-Learn* to perform the LGBM training, and hyperparameters of LGBM were tuned based on Grid Search Methods. The observed monthly human thermal indices from 2003 to 2020 at the 2419 weather stations across mainland China were randomly classified into a training set (80%) for hyperparameters tuning and model training and a testing set (20%) for model evaluation.

3.3 Accuracy assessment

Four statistic metrics, namely, determination coefficient (R^2), Mean Absolute Error (*MAE*), *RMSE*, and *Bias,* were used to evaluate the prediction accuracy of the human thermal indices. Ranging from 0 to 1, R^2 measures the proportion of variance explained by the model, representing how well the human thermal indicators were predicted compared to the observations. *MAE* represents the average absolute error between the predictions and the observations. *RMSE* is the standard deviation of the residuals and is sensitive to outliers. *Bias* describes the differences between the predictions and the observations. These metrics are computed as follows.

$$MAE = \frac{1}{N} \times \sum_{i=1}^{N} |y_i - \hat{y}| \tag{3}$$

$$RMSE = \sqrt{\frac{1}{N} \times \sum_{i=1}^{N} (y_i - \hat{y})^2} \tag{4}$$

$$R^2 = 1 - \frac{\sum_{i=1}^{N} (y_i - \hat{y})^2}{\sum_{i=1}^{N} (y_i - \bar{y})^2} \tag{5}$$

$$Bias = \frac{1}{N} \times \sum_{i=1}^{N} (y_i - \hat{y}) \tag{6}$$

where $\hat{y}$ is the predicted value of human thermal indices, $\bar{y}$ is the mean of the observed human thermal indices calculated from meteorological stations, and N is the number of samples.

4 Results

4.1 Evaluation of the prediction of human thermal indices

4.1.1 Overall accuracy

The prediction accuracies of the 12 human thermal indices were evaluated based on the validation data introduced in Section 3.2. All predicted human thermal indices exhibit high accuracies. Figure 2 shows

https://doi.org/10.5194/essd-2022-257
Preprint. Discussion started: 11 August 2022

the scatter plots of the observed versus the predicted values of 12 human thermal indices. As the figure displays, the data points of all indices are concentrated around the corresponding 1:1 line, indicating a good consistency between the observed and the predicted values. Figure 3 and Table S2 present the R^2, *MAE*, *RMSE,* and *Bias* values of 12 thermal indices from 2003 to 2020. The R^2 values of the 12 indices are all higher than 0.99, and their *RMSE*, *MAE,* and *Bias* are lower than 0.9 °C, 0.7 °C, and 0.003 °C, respectively. Particularly, HMI has the highest *RMSE* and *MAE* values, i.e., 0.859 °C and 0.645 °C, respectively; while ET shows the lowest *RMSE* and *MAE*, i.e., 0.377 °C and 0.281 °C, respectively. The larger error in terms of relatively higher RMSE and MAE for NET is likely caused by the incorporation of wind speed in computing this thermal indicator (see Table 2). These overall accuracies demonstrate that 12 human thermal indices predicted in this study are of good quality.

The spatial distributions of $R^{2,}$ *MAE, RMSE*, and *Bias* at individual stations across mainland China are depicted in Figure 4~7, respectively. The predicted indices have high R^2 values (i.e., >0.98, Figure 4) in almost all stations across China, demonstrating the superiority of LGBM. Better predictions in terms of higher R^2 are distributed in eastern China, particularly in the North China Plain (NCP) and the Yangtze River Delta (YRD), while southwestern China (e.g., the Yunnan-Guizhou Plateau (YGP)) has relatively lower R2 values (<0.98). For *MAE* and *RMSE*, all indices have small values <1 °C at most stations across China. *MAE* and *RMSE* show similar patterns, which exhibit the highest values in HMI (Figure 5g and 6g), followed by NET and WCT, and ET has the lowest *MAE* and *RMSE* values (i.e., < 0.4 °C, Figure 5e and 6e). The *MAE* and *RMSE* of NET and WCT decrease from northwestern to southeastern China (Figure 5i, 5l, 6i, 6l). For other indices, small *MAE* and *RMSE* values are mainly observed in plain regions including NCP, while high values tend to appear in regions with complex topography, such as arid Northwest China, mountainous Northeast and South China, and the Hengduan Mountains. This difference is related to the uneven distribution of weather stations, i.e., dense in plain areas and coarse in complex terrain areas. The *Bias* values range from -0.3 °C to 0.3 °C (Figure 7). Positive *Bias* values are mainly distributed in northern China, while negative *Bias* is seen in the south.

https://doi.org/10.5194/essd-2022-257
Preprint. Discussion started: 11 August 2022

4.1.2 Annual and monthly accuracies

The accuracies in terms of *RMSE*, *MAE,* and *Bias* of the 12 human thermal indices in individual years from 2003 to 2020 are assessed in Figure 8. *RMSEs* and *MAEs* of all indices in nearly all years are less than 1.0 °C (Figure 8a-b). Yearly *RMSE* (*MAE)* of ET fluctuates around 0.3 °C (0.2 °C) from 2003 to 2020. *RMSEs* (*MAEs)* of other indices range from 0.5 to 1.1 °C (0.4~0.8 °C) with marginal variations from year to year. *Biases* vary between -0.04 °C and 0.04 °C across all years. *Biases* seem to be slightly positive in 2003, 2004, and 2014 and negative in 2012, 2017, and 2018. Moreover, Figure S1 shows the *RMSEs*, *MAEs,* and *Biases* of all human thermal indices in different months. In terms of *RMSE*, all the indices in 12 months are lower than 1.4 °C, and their *MAEs* are less than 1 °C. HI and HMI have relatively higher *RMSE* and *MAE* values in summer than in other seasons; whereas, other indices tend to have larger errors in winter than in summer. Additionally, the magnitude of *Bias* is smaller than 0.03 °C for all the indices in 12 months.

4.1.3 Accuracies in major urban agglomerations

More than half of the national population in China lives in cities, particularly in UAs (i.e., also known as city clusters). Here we assessed the prediction accuracies in 20 major UAs in China, which hold 62.83% and 80.57% of the total population and gross domestic product (GDP) of the country (Fang, 2016). These accuracy assessments are presented in Tables S3~S6. As shown in Table S3, all UAs have the R^2 values higher than 0.9837, with an average of 0.9947. Table S4 also shows that these UAs have small *RMSE* values, most of which are smaller than 1 °C, except for the UA of North Tianshan Mountain in arid Northwest China. As the biggest UA in China, YRD has the lowest *RMSE* of 0.288 °C among all 20 UAs. The *MAEs* of the thermal indicators in all UAs are smaller than 1 °C and with an average value of 0.477 °C (Table S5). The *Biases* in the 20 UAs range from -0.160 °C to 0.123 °C (Table S6). These results suggest that all predicted human thermal indices in different UAs across China are of good quality at the local scale. It implies that our prediction model and results have great potential in evaluating local thermal environment changes (e.g., in urban areas or cities).

https://doi.org/10.5194/essd-2022-257
Preprint. Discussion started: 11 August 2022

4.2 Spatial variations of the human thermal indices

The abovementioned assessments show that our model based on LGBM can yield high-accuracy predictions at both national and local scales. Therefore, this model is employed to generate a high-resolution human thermal index collection at a monthly scale over China (HiTIC-Monthly) from 2003 to 2020. By taking monthly ET in 2020 as an example, we examined the monthly evolution of spatial patterns of the HiTIC-Monthly dataset in this subsection.

Figure 9 shows the monthly distribution of the predicted ET in 2020, which exhibits obvious seasonality with higher temperatures in summer and lower in winter. The temperature shows a significant zonal difference with colder temperature in northern than southern China. Temperature has a close relationship with topography and decreases with elevation, varying from plateaus to plains. The Qinghai-Tibet Plateau (TP) has the lowest temperature, while southern China, the Sichuan Basin, and the Gobi regions in Northwest China witness the highest temperature. The distribution of temperature exhibits different patterns among the four seasons, especially between winter (e.g., January) and summer (e.g., July). In winter, the temperature increases from northern to southern areas and is the coldest in Northeast and Northwest China and the warmest on the Hainan Island. In summer, the hottest temperature appears in the Tarim and Jungar Basins of Xinjiang. The NCP region also has a high temperature in summer, which might be related to local urbanization (Liu et al., 2008) and irrigation (Kang and Eltahir, 2018).

The spatial variations of the predicted human thermal indices in summer (which is often characterized by severe heat stress) are examined in Figure 10 by taking July 2020 as an example. As it shows, 12 indictors show similar distribution patterns. There are significant differences in temperature among northwest, northeast, and southeast. Generally, the temperature decreases from the southeast to the northwest, and the southeast and northwest parts have the highest and lowest temperature, respectively. HMI exhibits the highest temperature while NET shows the lowest in July 2020.

4.3 Temporal changes in the human thermal indices

The yearly evolutions of the annual mean human thermal indices during 2003~2020 are displayed in Figure 11. Despite the interannual fluctuation in the time series, all indicators exhibit upward trends

https://doi.org/10.5194/essd-2022-257
Preprint. Discussion started: 11 August 2022

except for NET and WCT, of which the decreasing trends are mainly affected by the recovering wind speed in the recent decade (Zeng et al., 2019). The fastest warming appears in HMI (0.303 °C/decade), and the slowest is in ET (0.111 °C/decade). These warming trends are stronger than the rising rate of global mean near surface temperature (IPCC, 2021), demonstrating China as one of the severest hotspots suffering from dramatic climate warming under global change. The detailed spatial variations regarding the trends of the human thermal indices across China are further depicted in Figure 12. Most parts of China experience increases in nearly all the indicators during 2003~2020. These increases are especially more profound in North China, Southwest China, TP, and parts of Northwest China. The possible reasons for the prominent warming trends in North China are explained as follows. The urbanization process has been prevailing in this area, with rapid growth in the economy and population. This process is accompanied by dramatic increases in impervious surfaces and decreases in green spaces. These changes lead to warmer surface and near surface air temperature, known as urban heat islands (UHI), thus increasing thermal stress in this region. The urbanization effects on local heat stress have also been reported by (Luo and Lau, 2021). Moreover, North China has a large amount of croplands with prominent irrigation activities, which may increase air humidity near the surface and exacerbate the combined effects of temperature and humidity, leading to increased heat stress (Kang and Eltahir, 2018). In addition, this area has experienced a weakening of surface wind speed (Zhang et al., 2021), which also exacerbates thermal stress, especially in NET and WCT.

Furthermore, different indices have different degrees of increasing trends. HMI has the largest increasing magnitude (Figure 12h), and ET is seen with relatively slight increases across China (Figure 12f). The trends of NET and WCT have similar spatial distribution patterns, with large proportions having cooling trends since 2003 (Figure 12j&l). Most parts of Xinjiang, northeastern and southern China have obvious decreasing trends, and the Inner Mongolia Plateau (IMP), NCP, eastern TP, YRD, and YGP have slight increasing trends.

The temporal trends of the human thermal indices in different seasons were also examined (Figure 13). The fastest warming tendency is observed in the spring season. The rising trends of spring HMI, HI, MDI, AT_{in}, and AT_{out} exceed 0.4 °C/decade, and the trends of other indices (except ET and NET) are larger

https://doi.org/10.5194/essd-2022-257
Preprint. Discussion started: 11 August 2022

than 0.3 °C/decade (Figure S2). Summer also has been experiencing significant increasing trends in all indicators, i.e., at a rate of > 0.2 °C/decade (except ET and NET). The trends in summer HMI, HI, WBT, MDI, DI, sWBGT, AT_{in}, and AT_{out} exceed 0.3 °C/decade (Figure S3). Differ from spring and summer, the human thermal indicators (except WCT and NET) in the autumn season show slightly cooling trends (Figure S4). Autumn WCT and NET have significantly strong decreasing trends, i.e., -0.349 and -0.507 °C/decade, respectively. Similar strong cooling trends of WCT and NET appear in winter, i.e., -0.661 and -0.453 °C/decade, respectively, while other indicators experience marginal long-term changes (Figure S5).

Figure S6 maps the spatial patterns of the trends of summer mean human thermal indices over mainland China during 2003~2020. All indicators show warming trends in most parts of China, particularly in NCP and TP. As one of the most densely populated regions in China, the prominent increases in thermal indices in NCP indicate that people living there have been experiencing increasing threats of intensifying heat stress. Among the 12 indicators, AT_{out}, HI, NET and WCT tend to have a slight cooling trend in southeastern China. This cooling trend is consistent with the corresponding summer SAT.

The spatial distributions of the changing trends in winter across mainland China during 2003~2020 are depicted in Figure S7. The trend patterns in winter are similar to that in summer to some degrees. The warming trends are concentrated in Southwest China, most parts of Northwest China, and parts of East China (e.g., YRD). The cooling trends are located in TP, parts of Northeast and South China. The cooling tendencies are especially profound in NET and WCT (Figures S7j&m), Northeast China, and most parts of Northwest and South China. Parts of central China are seen with even stronger cooling thermal comfort. In spring, increases in all thermal indicators are observed in most parts of China (Figure S8), particularly in northern regions, such as central Inner Mongolia, parts of NCP, and Northeast China, while parts of southern China have slight decreases. These decreases are noticeable in NET and WCT (Figures S8j&m). In contrast to spring, the autumn season is observed with decreased thermal temperature in the north and increases in the south (e.g., Southwest China, Figure S9).

https://doi.org/10.5194/essd-2022-257
Preprint. Discussion started: 11 August 2022

5 Discussion

5.1 Comparison with existing human thermal indices datasets

Our 1 km×1 km HITIC-Monthly product is compared with two existing datasets, HDI (Mistry, 2020) and HiTiSEA (Yan et al., 2021), which have coarser spatial resolutions of 0.25°×0.25° and 0.1°×0.1° (Figure S1), respectively. We derived monthly mean AT_{in} in July 2018 from the HDI and HiTiSEA, and compare them with our HITIC-Monthly over mainland China, with a particular highlight in the four largest UAs, including Beijing-Tianjin-Hebei (BTH), YRD, middle Yangtze River Valley (mYRV) and Pearl River Delta (PRD) (Figure 14). The summer of 2018 is selected by considering that it was included in all three datasets and frequent heat events occurred in this summer (Zhou et al., 2020). Generally, the three datasets depict similar spatial patterns. However, our HiTIC-Monthly dataset obviously provides more detailed and clearer spatial information on human thermal stress than the other two. Additionally, the observed AT_{in} values at individual weather stations are also compared in Figure 14. It can be seen that HDI and HiTISEA overestimate AT_{in}, and such overestimation is especially severe in HDI; whereas our dataset is in good agreement with the observed AT_{in} at individual weather stations. Therefore, our predicted temperature can describe the spatial variations in the city areas well, thereby providing fundamental support for fine-scale climate studies, such as urban climate research.

5.2 Limitations and future works

There are 12 commonly used human thermal indices in the HiTIC-Monthly dataset produced in this study. Nine of these indices were computed from temperature and humidity (or water vapor) and the other three (i.e., AT_{out}, NET, and WCT) were derived from temperature, humidity, and wind speed. In addition, by considering the combined effect of environmental variables, some other indices have been proposed in the literature, such as sunlight (Blazejczyk, 1994; Fanger, 1970; Höppe, 1999; Yaglou and Minaed, 1957). These indices include wet bulb globe temperature (WBGT), predicted mean vote (PMV), UTCI, physiological equivalent temperature (PET), etc. These thermal indices are not included in our study due to the lack of sunshine and radiative flux data.

Since LST is the most important variable for predicting the human thermal indices, the uncertainty in the LST dataset may harm the accuracy of the human thermal indices. The LST variable in our prediction is

https://doi.org/10.5194/essd-2022-257
Preprint. Discussion started: 11 August 2022

Open Access Earth System Science Data Discussions

from a global seamless 1 km resolution daily LST dataset (Zhang et al., 2022b). This dataset was generated based on spatiotemporal gap-filling algorithms and the MODIS LST dataset. It may overestimate LST in some cases because the LST under cloudy weather was filled based on the data under clear sky conditions (Zhang et al., 2022b). A high-quality LST dataset would further improve the prediction accuracy of the human thermal indices.

The human thermal indices dataset is at a monthly scale, but the temporal resolution may not be sufficient for the research of extreme weather events (e.g., heatwaves) and related environmental health (e.g., heat-related mortality). A dataset of high spatial resolution daily human thermal index collection (HiTIC-Daily) will be produced and released in our future studies. In the current study, we provided the first national multiple monthly human thermal indices dataset over the mainland of China, and this dataset shows high prediction accuracies in all climate regimes across China. A global dataset of multiple human thermal indices dataset is also expected in the near future.

6 Data availability

The high spatial resolution monthly human thermal index collection (HiTIC-Monthly) generated in this study is freely available to the public in network common data form (NetCDF) at https://zenodo.org/record/6895533 (Zhang et al., 2022a). The human thermal indices include surface air temperature (SAT), indoor Apparent Temperature (AT_{in}), outdoor shaded Apparent Temperature (AT_{out}), Discomfort Index (DI), Effective Temperature (ET), Heat Index (HI), Humidex (HMI), Modified Discomfort Index (MDI), Net Effective Temperature (NET), simplified Wet Bulb Globe Temperature (sWBGT), Wet-Bulb Temperature (WBT), and Wind Chill Temperature (WCT). This dataset has a spatial resolution of 1 km×1 km and covers mainland China from January 2003 to December 2020, stacking by year. Each stack is composed of 12 monthly images. The unit of the dataset is 0.01 degree Celsius (°C), and the projection coordinate system is Albers Equal Area Conic Projection. The naming rule and other detailed information can be found in “README.pdf”.

7 Conclusions

A long-term and high-resolution dataset of multiple human thermal indices is of great significance for studying detailed spatial and temporal changes of human thermal stress in different climate regions across China and assessing the health risks of people exposed to extreme heat at a fine scale. However, the current datasets of human thermal indices (e.g., HDI and HiTiSEA) only have coarse spatial resolutions (> 0.1°). In this study, we generated a dataset of monthly human thermal index collection with a high spatial resolution of 1 km×1 km over mainland China (HiTIC-Monthly). In this collection, twelve human thermal indicators were predicted, including SAT, AT_{in}, AT_{out}, DI, ET, HI, HMI, MDI, NET, sWBGT, WBT, and WCT, from January 2003 to December 2020.

The HiTIC-Monthly dataset was produced by LGBM based on multi-source grided data, including MODIS LST, DEM, land cover and land use, population density, and impervious surface fraction. This dataset shows a desirable performance, with mean R^2, *RMSE*, *MAE,* and *Bias* of 0.996, 0.693°C, 0.512°C, and 0.003°C, respectively. Our predictions also exhibit good agreements with the observations in both spatial and temporal dimensions, demonstrating the broad applicability of our dataset. Moreover, the comparison with two existing datasets (i.e., HDI and HiTiSEA) suggests that HiTIC-Monthly has more detailed spatial information, indicating that our dataset can well support fine-scale studies. Further investigation shows that almost all the indicators show warming trends in most parts of China during 2003~2020, particularly for North China, Southwest China, TP, and parts of Northwest China. Additionally, the warming tendency is faster in the spring and summer seasons. WCT and NET show similar and strong cooling trends in autumn and winter, while other indicators exhibit slight long-term changes.

Author contribution

H.Z.: Data curation, Formal analysis, Investigation, Methodology, Writing – original draft preparation; M.L.: Conceptualization, Investigation, Funding acquisition Methodology, Supervision Writing – review & editing; Y.Z.: Investigation, Supervision Writing – review & editing; L.J.: Investigation, Writing – review & editing; E.G.: Investigation, Writing – review & editing; Y.Y.: Investigation, Writing – review

& editing; G.N.: Investigation, Writing – review & editing; J.G.: Investigation, Writing – review & editing; Z.Z. Investigation, Writing – review & editing; K.G.: Investigation, Writing – review & editing; J.L.: Investigation, Writing – review & editing; X.L.: Investigation, Writing – review & editing; S.W.: Investigation, Writing – review & editing; P.W.: Investigation, Writing – review & editing; X.W.: Investigation, Writing – review & editing.

Competing interests

The authors declare that they have no conflict of interest.

Acknowledgments

This work was supported by the National Natural Science Foundation of China (41871029), the National Key R&D Program of China (2019YFC1510400), the Natural Science Foundation of Guangdong Province, China (2019A1515011025), and the Pearl River Talent Recruitment Program of Guangdong Province (2017GC010634).

References

Abatzoglou, J. T., Dobrowski, S. Z., Parks, S. A., and Hegewisch, K. C.: TerraClimate, a high-resolution global dataset of monthly climate and climatic water balance from 1958-2015, Sci Data, 5, 170191, https://doi.org/10.1038/sdata.2017.191, 2018.

Arias, P., Bellouin, N., Coppola, E., Jones, R., Krinner, G., Marotzke, J., Naik, V., Palmer, M., Plattner, G.-K., and Rogelj, J.: Climate Change 2021: The Physical Science Basis. Contribution of Working Group14 I to the Sixth Assessment Report of the Intergovernmental Panel on Climate Change; Technical Summary, 2021.

Blazejczyk, K.: New climatological-and-physiological model of the human heat balance outdoor (MENEX) and its applications in bioclimatological studies in different scales, Zeszyty IgiPZ PAN, 28, 27-58, 1994.

Brake, R. and Bates, G.: A valid method for comparing rational and empirical heat stress indices, The Annals of Occupational Hygiene, 46, 165-174, https://doi.org/10.1093/annhyg/mef030, 2002.

Brimicombe, C., Di Napoli, C., Cornforth, R., Pappenberger, F., Petty, C., and Cloke, H. L.: Borderless Heat Hazards With Bordered Impacts, Earth's Future, 9, https://doi.org/10.1029/2021ef002064, 2021.

Budhathoki, N. K. and Zander, K. K.: Socio-Economic Impact of and Adaptation to Extreme Heat and

https://doi.org/10.5194/essd-2022-257
Preprint. Discussion started: 11 August 2022

Cold of Farmers in the Food Bowl of Nepal, International Journal of Environmental Research and Public Health, 16, https://doi.org/10.3390/ijerph16091578, 2019.

Candido, C., Blanco, A. C., Medina, J., Gubatanga, E., Santos, A., Ana, R. S., and Reyes, R. B.: Improving the consistency of multi-temporal land cover mapping of Laguna lake watershed using light gradient boosting machine (LightGBM) approach, change detection analysis, and Markov chain, Remote Sensing Applications: Society and Environment, 23, https://doi.org/10.1016/j.rsase.2021.100565, 2021.

Di Napoli, C., Pappenberger, F., and Cloke, H. L.: Assessing heat-related health risk in Europe via the Universal Thermal Climate Index (UTCI), International Journal of Biometeorology, 62, 1155-1165, https://doi.org/10.1007/s00484-018-1518-2, 2018.

Di Napoli, C., Barnard, C., Prudhomme, C., Cloke, H. L., and Pappenberger, F.: ERA5-HEAT: A global gridded historical dataset of human thermal comfort indices from climate reanalysis, Geoscience Data Journal, 8, 2-10, https://doi.org/10.1002/gdj3.102, 2020.

Djongyang, N., Tchinda, R., and Njomo, D.: Thermal comfort: A review paper, Renewable and Sustainable Energy Reviews, 14, 2626-2640, https://doi.org/10.1016/j.rser.2010.07.040, 2010.

ECMWF: Copernicus Climate Change Service (C3S): ERA5: Fifth generation of ECMWF atmospheric reanalyses of the global climate. Copernicus Climate Change Service Climate Data Store (CDS), 2017.

Enander, A. E. and Hygge, S.: Thermal stress and human performance, Scand J Work Environ Health, 16 Suppl 1, 44-50, https://doi.org/10.5271/sjweh.1823, 1990.

Epstein, Y. and Moran, D. S.: Thermal comfort and the heat stress indices, Ind Health, 44, 388-398, https://doi.org/10.2486/indhealth.44.388, 2006.

Fan, J., Ma, X., Wu, L., Zhang, F., Yu, X., and Zeng, W.: Light Gradient Boosting Machine: An efficient soft computing model for estimating daily reference evapotranspiration with local and external meteorological data, Agricultural Water Management, 225, https://doi.org/10.1016/j.agwat.2019.105758, 2019.

Fang, C.: China's New Urbanization Developmental Paths, Blueprints and Patterns/Chuanglin Fang, Danlin Yu, 2016.

Fanger, P. O.: Thermal comfort. Analysis and applications in environmental engineering, Thermal comfort. Analysis and applications in environmental engineering., 1970.

Gagge, A. and Nishi, Y.: Physical indices of the thermal environment, ASHRAE J.;(United States), 18, 1976.

Gagge, A., Stolwijk, J. A., and Nishi, Y.: An effective temperature scale based on a simple model of human physiological regulatiry response, Memoirs of the Faculty of Engineering, Hokkaido University, 13, 21-36, 1972.

Gaughan, A. E., Stevens, F. R., Linard, C., Jia, P., and Tatem, A. J.: High resolution population distribution maps for Southeast Asia in 2010 and 2015, PLoS One, 8, e55882, https://doi.org/10.1371/journal.pone.0055882, 2013.

Gong, P., Li, X., Wang, J., Bai, Y., Chen, B., Hu, T., Liu, X., Xu, B., Yang, J., Zhang, W., and Zhou, Y.: Annual maps of global artificial impervious area (GAIA) between 1985 and 2018, Remote Sensing of Environment, 236, https://doi.org/10.1016/j.rse.2019.111510, 2020.

Haines, A. and Ebi, K.: The Imperative for Climate Action to Protect Health, The New England Jornal of Medicine, 380, 263-273, https://doi.org/10.1056/NEJMra1807873, 2019.

He, Q., Wang, M., Liu, K., Li, K., and Jiang, Z.: GPRChinaTemp1km: a high-resolution monthly air temperature dataset for China (1951–2020) based on machine learning, Earth System Science Data Discussions, 1-29, 2021.

Hong, F., Zhan, W., Göttsche, F.-M., Liu, Z., Dong, P., Fu, H., Huang, F., and Zhang, X.: A global dataset of spatiotemporally seamless daily mean land surface temperatures: generation, validation, and analysis, Earth System Science Data, 14, 3091-3113, https://doi.org/10.5194/essd-14-3091-2022, 2022.

Höppe, P.: The physiological equivalent temperature–a universal index for the biometeorological assessment of the thermal environment, International journal of Biometeorology, 43, 71-75, 1999.

Houghton, F. C. and Yaglou, C. P.: Determining equal comfortlines, ASHVE Trans., 29, 165-176, 1923.

IPCC: Climate Change 2021: The Physical Science Basis. Contribution of Working Group I to the Sixth Assessment Report of the Intergovernmental Panel on Climate Change, 2021.

Kang, S. and Eltahir, E. A. B.: North China Plain threatened by deadly heatwaves due to climate change and irrigation, Nature Communications, 9, 2894, https://doi.org/10.1038/s41467-018-05252-y, 2018.

Ke, G., Meng, Q., Finley, T., Wang, T., Chen, W., Ma, W., Ye, Q., and Liu, T.-Y.: Lightgbm: A highly efficient gradient boosting decision tree, Advances in neural information processing systems, 30, 2017.

Krzysztof, B., Pavol, N., Oleh, S., Agnieszka, H., Olesya, S., Anna, B., and Katarina, M.: Influence of geographical factors on thermal stress in northern Carpathians, International Journal of Biometeorology, 65, 1553-1566, https://doi.org/10.1007/s00484-020-02011-x, 2021.

Kuchcik, M.: Mortality and thermal environment (UTCI) in Poland-long-term, multi-city study, International Journal of Biometeorology 65, 1529-1541, https://doi.org/10.1007/s00484-020-01995-w, 2021.

Lazaro, P. and Momayez, M.: Heat Stress in Hot Underground Mines: a Brief Literature Review, Mining, Metallurgy & Exploration, 38, 497-508, https://doi.org/10.1007/s42461-020-00324-4, 2020.

Li, J., Chen, Y. D., Gan, T. Y., and Lau, N.-C.: Elevated increases in human-perceived temperature under climate warming, Nature Climate Change, 8, 43-47, https://doi.org/10.1038/s41558-017-0036-2, 2018.

Li, Q., Liu, X., Zhang, H., Thomas C, P., and David R, E.: Detecting and adjusting temporal inhomogeneity in Chinese mean surface air temperature data, Advances in Atmospheric Sciences, 21, 260-268, https://doi.org/10.1007/bf02915712, 2004.

Li, W., Hao, X., Wang, L., Li, Y., Li, J., Li, H., and Han, T.: Detection and Attribution of Changes in Thermal Discomfort over China during 1961–2014 and Future Projections, Advances in Atmospheric Sciences, 39, 456-470, https://doi.org/10.1007/s00376-021-1168-x, 2022.

Liu, X., Guo, J., Zhang, A., Zhou, J., Chu, Z., Zhou, Y., and Ren, G.: Urbanization Effects on Observed Surface Air Temperature Trends in North China, Journal of Climate, 21, 1333-1348, https://doi.org/10.1175/2007jcli1348.1, 2008.

Los, H., Mendes, G. S., Cordeiro, D., Grosso, N., Costa, H., Benevides, P., and Caetano, M.: Evaluation of Xgboost and Lgbm Performance in Tree Species Classification with Sentinel-2 Data, 2021 IEEE International Geoscience and Remote Sensing Symposium IGARSS, https://doi.org/10.1109/igarss47720.2021.9553031, 2021.

Luo, M. and Lau, N.-C.: Characteristics of summer heat stress in China during 1979–2014: climatology and long-term trends, Climate Dynamics, 53, 5375-5388, https://doi.org/10.1007/s00382-019-04871-5, 2019.

Luo, M. and Lau, N. C.: Increasing Human-Perceived Heat Stress Risks Exacerbated by Urbanization in

https://doi.org/10.5194/essd-2022-257
Preprint. Discussion started: 11 August 2022

China: A Comparative Study Based on Multiple Metrics, Earth's Future, 9, https://doi.org/10.1029/2020ef001848, 2021.

Luo, M., Lau, N. C., Liu, Z., Wu, S., and Wang, X.: An Observational Investigation of Spatiotemporally Contiguous Heatwaves in China From a 3D Perspective, Geophysical Research Letters, 49, https://doi.org/10.1029/2022gl097714, 2022.

Masterton, J. M., Richardson, F. A., and atmosphérique, C. S. d. l. e.: Humidex: A Method of Quantifying Human Discomfort Due to Excessive Heat and Humidity, Service de l'environnement atmospherique. 1979.

McCarty, D. A., Kim, H. W., and Lee, H. K.: Evaluation of Light Gradient Boosted Machine Learning Technique in Large Scale Land Use and Land Cover Classification, Environments, 7, https://doi.org/10.3390/environments7100084, 2020.

Mistry, M. N.: A High Spatiotemporal Resolution Global Gridded Dataset of Historical Human Discomfort Indices, Atmosphere, 11, https://doi.org/10.3390/atmos11080835, 2020.

Moda, H. M., Filho, W. L., and Minhas, A.: Impacts of Climate Change on Outdoor Workers and their Safety: Some Research Priorities, International Journal of Environmental Research and Public Health, 16, https://doi.org/10.3390/ijerph16183458, 2019.

Moran, D., Shapiro, Y., Epstein, Y., Matthew, W., and Pandolf, K.: A modified discomfort index (MDI) as an alternative to the wet bulb globe temperature (WBGT), Environmental Ergonomics VIII, Hodgdon JA, Heaney JH, Buono MJ (Eds.), 77-80, 1998.

Nastos, P. T. and Matzarakis, A.: The effect of air temperature and human thermal indices on mortality in Athens, Greece, Theoretical and Applied Climatology, 108, 591-599, https://doi.org/10.1007/s00704-011-0555-0, 2011.

NWS: Meteorological Conversions and Calculations: Heat Index Calculator, 2011.

Osczevski, R. and Bluestein, M.: The New Wind Chill Equivalent Temperature Chart, Bulletin of the American Meteorological Society, 86, 1453-1458, https://doi.org/10.1175/bams-86-10-1453, 2005.

Patz, J. A., Campbell-Lendrum, D., Holloway, T., and Foley, J. A.: Impact of regional climate change on human health, Nature, 438, 310-317, https://doi.org/10.1038/nature04188, 2005.

Peng, S., Ding, Y., Liu, W., and Li, Z.: 1 km monthly temperature and precipitation dataset for China from 1901 to 2017, Earth System Science Data, 11, 1931-1946, https://doi.org/10.5194/essd-11-1931-2019, 2019.

Periard, J. D., Eijsvogels, T. M. H., and Daanen, H. A. M.: Exercise under heat stress: thermoregulation, hydration, performance implications, and mitigation strategies, Physiol Rev, 101, 1873-1979, https://doi.org/10.1152/physrev.00038.2020, 2021.

Rahman, M. A., Franceschi, E., Pattnaik, N., Moser-Reischl, A., Hartmann, C., Paeth, H., Pretzsch, H., Rotzer, T., and Pauleit, S.: Spatial and temporal changes of outdoor thermal stress: influence of urban land cover types, Sci Rep, 12, 671, https://doi.org/10.1038/s41598-021-04669-8, 2022.

Raymond, C., Matthews, T., and Horton, R. M.: The emergence of heat and humidity too severe for human tolerance, Science Advances, 6, eaaw1838, https://doi.org/10.1126/sciadv.aaw1838, 2020.

Ren, Z., Fu, Y., Dong, Y., Zhang, P., and He, X.: Rapid urbanization and climate change significantly contribute to worsening urban human thermal comfort: A national 183-city, 26-year study in China, Urban Climate, 43, https://doi.org/10.1016/j.uclim.2022.101154, 2022.

Rogers, C. D. W., Ting, M., Li, C., Kornhuber, K., Coffel, E. D., Horton, R. M., Raymond, C., and Singh, D.: Recent Increases in Exposure to Extreme Humid-Heat Events Disproportionately Affect Populated Regions, Geophysical Research Letters, 48, https://doi.org/10.1029/2021gl094183, 2021.

https://doi.org/10.5194/essd-2022-257
Preprint. Discussion started: 11 August 2022

Roghanchi, P. and Kocsis, K. C.: Challenges in Selecting an Appropriate Heat Stress Index to Protect Workers in Hot and Humid Underground Mines, Saf Health Work, 9, 10-16, https://doi.org/10.1016/j.shaw.2017.04.002, 2018.

Rothfusz, L. P. and Headquarters, N. S. R.: The heat index equation (or, more than you ever wanted to know about heat index), Fort Worth, Texas: National Oceanic and Atmospheric Administration, National Weather Service, Office of Meteorology, 9023, 1990.

Rustemeyer, N. and Howells, M.: Excess Mortality in England during the 2019 Summer Heatwaves, Climate, 9, https://doi.org/10.3390/cli9010014, 2021.

Schwingshackl, C., Sillmann, J., Vicedo-Cabrera, A. M., Sandstad, M., and Aunan, K.: Heat Stress Indicators in CMIP6: Estimating Future Trends and Exceedances of Impact-Relevant Thresholds, Earth's Future, 9, https://doi.org/10.1029/2020ef001885, 2021.

Sohar, E., Adar, R., and Kaly, J.: Comparison of the environmental heat load in various parts of Israel, ISRAEL JOURNAL OF EXPERIMENTAL MEDICINE, 10, 111-&, 1963.

Staiger, H., Laschewski, G., and Matzarakis, A.: Selection of Appropriate Thermal Indices for Applications in Human Biometeorological Studies, Atmosphere, 10, https://doi.org/10.3390/atmos10010018, 2019.

Steadman, R. G.: The assessment of sultriness. Part I: A temperature-humidity index based on human physiology and clothing science, Journal of Applied Meteorology and Climatology, 18, 861-873, 1979.

Steadman, R. G.: A universal scale of apparent temperature, Journal of Applied Meteorology and Climatology, 23, 1674-1687, 1984.

Stolwijk, J.: Heat exchangers between body and environment, Bibliotheca Radiologica, 144-150, 1975.

Stull, R.: Wet-Bulb Temperature from Relative Humidity and Air Temperature, Journal of Applied Meteorology and Climatology, 50, 2267-2269, https://doi.org/10.1175/jamc-d-11-0143.1, 2011.

Su, H., Wang, A., Zhang, T., Qin, T., Du, X., and Yan, X.-H.: Super-resolution of subsurface temperature field from remote sensing observations based on machine learning, International Journal of Applied Earth Observation and Geoinformation, 102, https://doi.org/10.1016/j.jag.2021.102440, 2021.

Su, Y.: Prediction of air quality based on Gradient Boosting Machine Method, 2020 International Conference on Big Data and Informatization Education (ICBDIE), https://doi.org/10.1109/icbdie50010.2020.00099, 2020.

Sulla-Menashe, D. and Friedl, M.: MCD12Q1 MODIS/Terra+ Aqua Land Cover Type Yearly L3 Global 500m SIN Grid V006, NASA EOSDIS Land Processes DAAC: Sioux Falls, SD, USA, https://doi.org/10.5067/MODIS/MCD12Q1.006, 2019.

Sun, Q., Miao, C., Hanel, M., Borthwick, A. G. L., Duan, Q., Ji, D., and Li, H.: Global heat stress on health, wildfires, and agricultural crops under different levels of climate warming, Environment International, 128, 125-136, https://doi.org/10.1016/j.envint.2019.04.025, 2019.

Szer, I., Lipecki, T., Szer, J., and Czarnocki, K.: Using meteorological data to estimate heat stress of construction workers on scaffolds for improved safety standards, Automation in Construction, 134, https://doi.org/10.1016/j.autcon.2021.104079, 2022.

Tamiminia, H., Salehi, B., Mahdianpari, M., Beier, C. M., Johnson, L., and Phoenix, D. B.: A Comparison of Random Forest and Light Gradient Boosting Machine for Forest above-Ground Biomass Estimation Using a Combination of Landsat, Alos Palsar, and Airborne Lidar Data, The International Archives of the Photogrammetry, Remote Sensing and Spatial Information Sciences, XLIV-M-3-2021, 163-168, https://doi.org/10.5194/isprs-archives-XLIV-M-3-2021-163-2021, 2021.

Tian, H., Zhao, Y., Luo, M., He, Q., Han, Y., and Zeng, Z.: Estimating PM2.5 from multisource data: A comparison of different machine learning models in the Pearl River Delta of China, Urban Climate, 35, https://doi.org/10.1016/j.uclim.2020.100740, 2021.

Tian, P., Lu, H., Li, D., and Guan, Y.: Quantifying the effects of meteorological change between neighboring days on human thermal comfort in China, Theoretical and Applied Climatology, 147, 1345-1357, https://doi.org/10.1007/s00704-021-03908-2, 2022.

Tong, S., Prior, J., McGregor, G., Shi, X., and Kinney, P.: Urban heat: an increasing threat to global health, BMJ, 375, n2467, https://doi.org/10.1136/bmj.n2467, 2021.

Tuholske, C., Caylor, K., Funk, C., Verdin, A., Sweeney, S., Grace, K., Peterson, P., and Evans, T.: Global urban population exposure to extreme heat, Proc Natl Acad Sci U S A, 118, https://doi.org/10.1073/pnas.2024792118, 2021.

United Nations: World population prospects, Multimedia Library, 2017.

Varentsov, M., Shartova, N., Grischenko, M., and Konstantinov, P.: Spatial Patterns of Human Thermal Comfort Conditions in Russia: Present Climate and Trends, Weather, Climate, and Society, 12, 629-642, https://doi.org/10.1175/wcas-d-19-0138.1, 2020.

Wang, C., Zhan, W., Liu, Z., Li, J., Li, L., Fu, P., Huang, F., Lai, J., Chen, J., Hong, F., and Jiang, S.: Satellite-based mapping of the Universal Thermal Climate Index over the Yangtze River Delta urban agglomeration, Journal of Cleaner Production, 277, https://doi.org/10.1016/j.jclepro.2020.123830, 2020.

Wang, F., Duan, K., and Zou, L.: Urbanization Effects on Human-Perceived Temperature Changes in the North China Plain, Sustainability, 11, https://doi.org/10.3390/su11123413, 2019.

Wang, P., Luo, M., Liao, W., Xu, Y., Wu, S., Tong, X., Tian, H., Xu, F., and Han, Y.: Urbanization contribution to human perceived temperature changes in major urban agglomerations of China, Urban Climate, 38, https://doi.org/10.1016/j.uclim.2021.100910, 2021.

Xu, W., Li, Q., Wang, X. L., Yang, S., Cao, L., and Feng, Y.: Homogenization of Chinese daily surface air temperatures and analysis of trends in the extreme temperature indices, Journal of Geophysical Research: Atmospheres, 118, 9708-9720, https://doi.org/10.1002/jgrd.50791, 2013.

Yaglou, C. and Minaed, D.: Control of heat casualties at military training centers, Arch. Indust. Health, 16, 302-316, 1957.

Yamazaki, D., Ikeshima, D., Tawatari, R., Yamaguchi, T., O'Loughlin, F., Neal, J. C., Sampson, C. C., Kanae, S., and Bates, P. D.: A high-accuracy map of global terrain elevations, Geophysical Research Letters, 44, 5844-5853, https://doi.org/10.1002/2017gl072874, 2017.

Yan, Y., Xu, Y., and Yue, S.: A high-spatial-resolution dataset of human thermal stress indices over South and East Asia, Sci Data, 8, 229, https://doi.org/10.1038/s41597-021-01010-w, 2021.

Yan, Y. Y.: Human Thermal Climates in China, Physical Geography, 26, 163-176, https://doi.org/10.2747/0272-3646.26.3.163, 2013.

Zeng, Z., Gui, K., Wang, Z., Luo, M., Geng, H., Ge, E., An, J., Song, X., Ning, G., Zhai, S., and Liu, H.: Estimating hourly surface PM2.5 concentrations across China from high-density meteorological observations by machine learning, Atmospheric Research, 254, https://doi.org/10.1016/j.atmosres.2021.105516, 2021.

Zeng, Z., Ziegler, A. D., Searchinger, T., Yang, L., Chen, A., Ju, K., Piao, S., Li, L. Z. X., Ciais, P., Chen, D., Liu, J., Azorin-Molina, C., Chappell, A., Medvigy, D., and Wood, E. F.: A reversal in global terrestrial stilling and its implications for wind energy production, Nature Climate Change, 9, 979-985, https://doi.org/10.1038/s41558-019-0622-6, 2019.

Zhang, G., Azorin-Molina, C., Chen, D., McVicar, T. R., Guijarro, J. A., Kong, F., Minola, L., Deng, K., and Shi, P.: Uneven Warming Likely Contributed to Declining Near-Surface Wind Speeds in Northern China Between 1961 and 2016, Journal of Geophysical Research: Atmospheres, 126, https://doi.org/10.1029/2020jd033637, 2021.

Zhang, H., Luo, M., Zhao, Y., Lin, L., Ge, E., Yang, Y., Ning, G., Zeng, Z., Gui, K., Li, J., Chen, T. O., Li, X., Wu, S., Wang, P., and Wang, X.: HiTIC-Monthly: A High Spatial Resolution (1 km×1 km) Monthly Human Thermal Index Collection over China from 2003 to 2020 (1.0), Zenodo [dataset], https://doi.org/10.5281/zenodo.6895533, 2022a.

Zhang, T., Zhou, Y., Zhu, Z., Li, X., and Asrar, G. R.: A global seamless 1 km resolution daily land surface temperature dataset (2003–2020), Earth System Science Data, 14, 651-664, https://doi.org/10.5194/essd-14-651-2022, 2022b.

Zhao, B., Mao, K., Cai, Y., Shi, J., Li, Z., Qin, Z., Meng, X., Shen, X., and Guo, Z.: A combined Terra and Aqua MODIS land surface temperature and meteorological station data product for China from 2003 to 2017, Earth System Science Data, 12, 2555-2577, https://doi.org/10.5194/essd-12-2555-2020, 2020.

Zhao, C., Liu, B., Piao, S., Wang, X., Lobell, D. B., Huang, Y., Huang, M., Yao, Y., Bassu, S., Ciais, P., Durand, J. L., Elliott, J., Ewert, F., Janssens, I. A., Li, T., Lin, E., Liu, Q., Martre, P., Muller, C., Peng, S., Penuelas, J., Ruane, A. C., Wallach, D., Wang, T., Wu, D., Liu, Z., Zhu, Y., Zhu, Z., and Asseng, S.: Temperature increase reduces global yields of major crops in four independent estimates, Proc Natl Acad Sci U S A, 114, 9326-9331, https://doi.org/10.1073/pnas.1701762114, 2017.

Zhao, Y. and Zhu, Z.: ASI: An artificial surface Index for Landsat 8 imagery, International Journal of Applied Earth Observation and Geoinformation, 107, 10.1016/j.jag.2022.102703, 2022.

Zhou, C., Chen, D., Wang, K., Dai, A., and Qi, D.: Conditional Attribution of the 2018 Summer Extreme Heat over Northeast China: Roles of Urbanization, Global Warming, and Warming-Induced Circulation Changes, Bulletin of the American Meteorological Society, 101, S71-S76, https://doi.org/10.1175/bams-d-19-0197.1, 2020.

https://doi.org/10.5194/essd-2022-257
Preprint. Discussion started: 11 August 2022

750 **Figures**

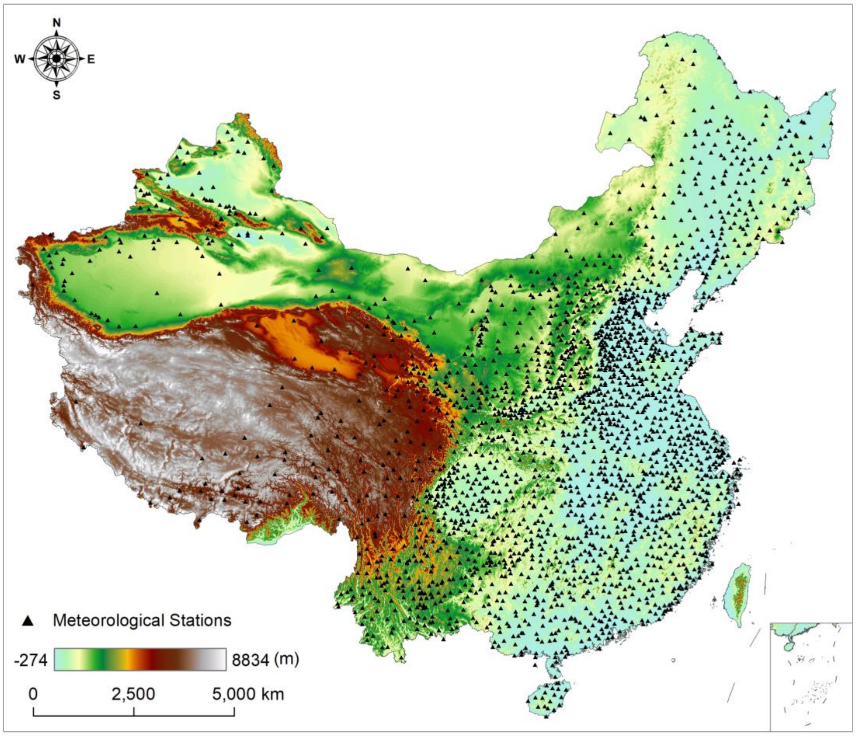

Figure 1. Spatial distribution of meteorological stations in the mainland of China, with color shadings indicating the elevation in meters.

https://doi.org/10.5194/essd-2022-257
Preprint. Discussion started: 11 August 2022

Open Access Earth System Science Data Discussions

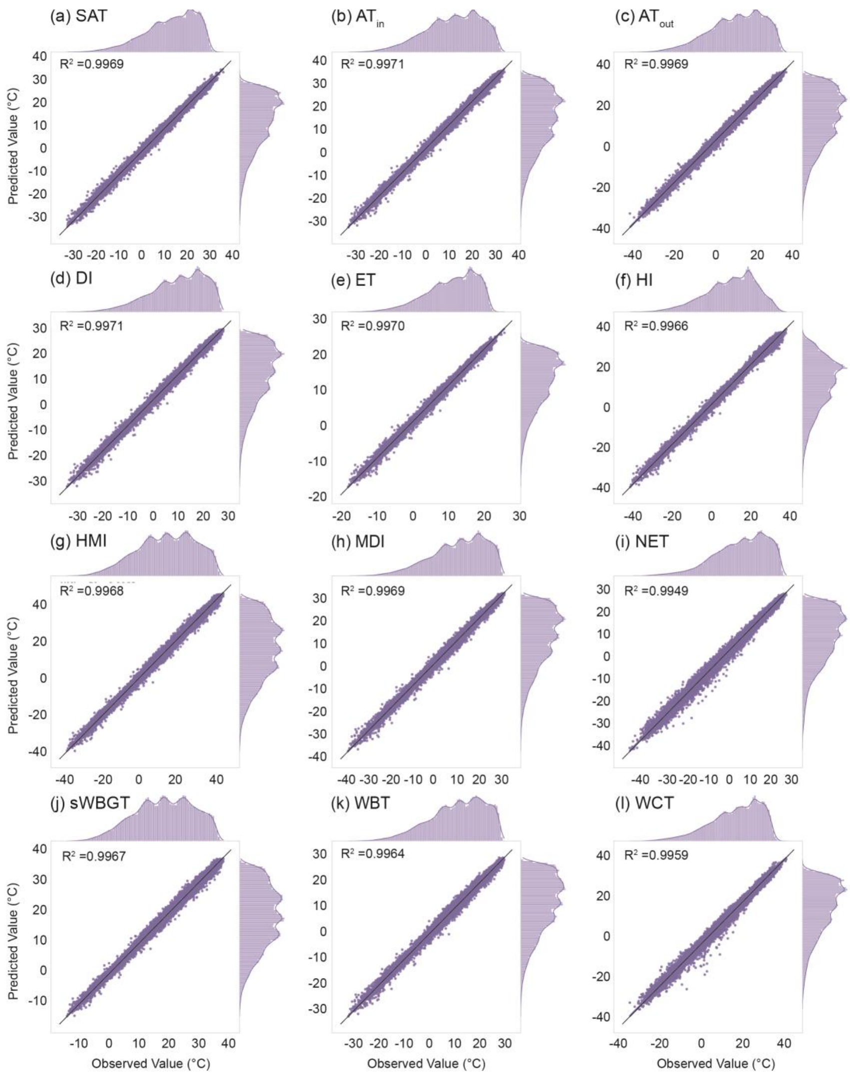

755 **Figure 2. Scatter plots of predicted versus observed values of 12 human thermal indices over mainland China during 2003~2020: (a) SAT, (b) AT_{in}, (c) AT_{out}, (d) DI, (e) ET, (f) HI, (g) HMI, (h) MDI, (i) NET, (j) sWBGT, (k) WBT, and (l) WCT. The black straight line is the 1:1 line.**

https://doi.org/10.5194/essd-2022-257
Preprint. Discussion started: 11 August 2022

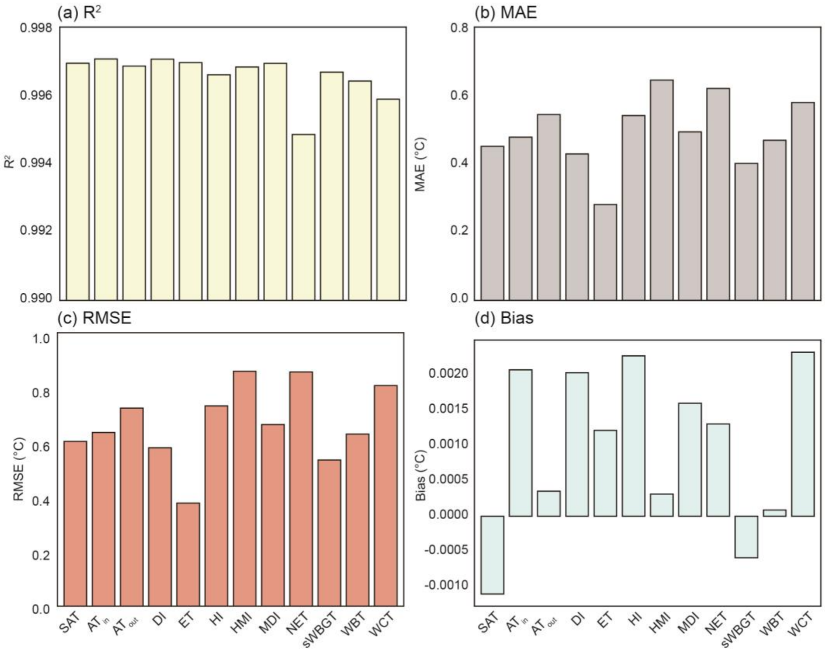

760 **Figure 3. Overall prediction accuracies of 12 human thermal indices over mainland China during 2003~2020: (a) R^2, (b) *MAE*, (c) *RMSE*, (d) *Bias*.**

https://doi.org/10.5194/essd-2022-257
Preprint. Discussion started: 11 August 2022

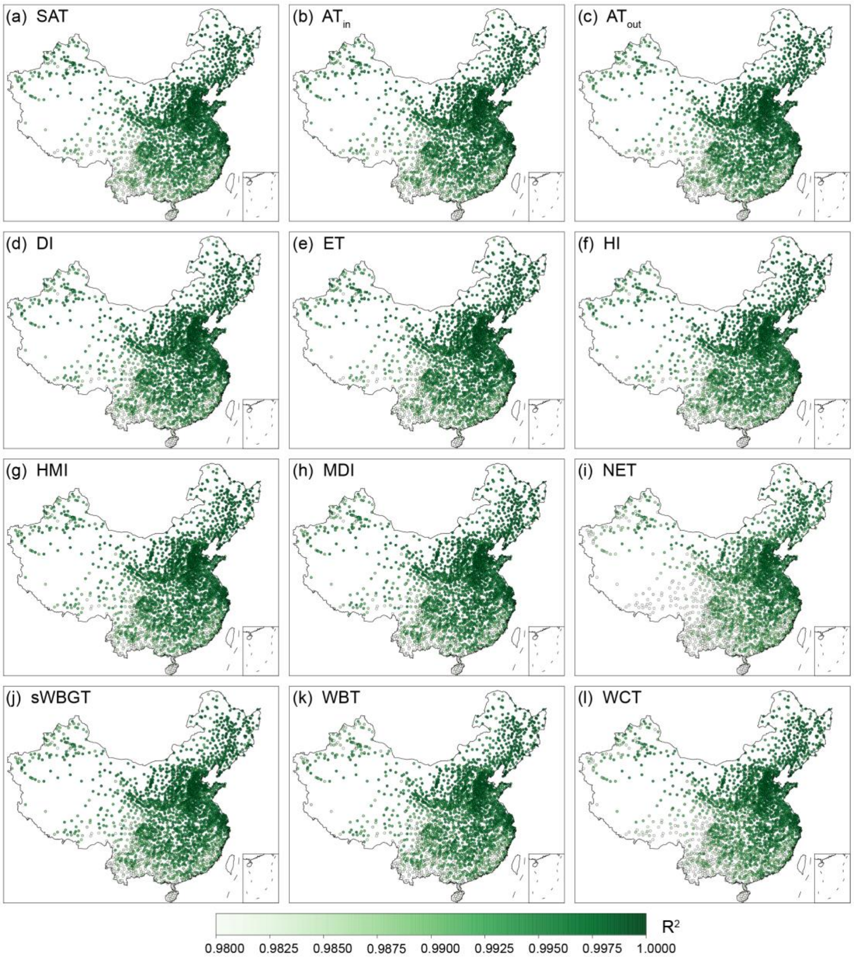

Figure 4. Spatial distribution of R^2 of the human thermal index predictions at individual meteorological stations over mainland China during 2003~2020.

https://doi.org/10.5194/essd-2022-257
Preprint. Discussion started: 11 August 2022

Open Access Earth System Science Data Discussions

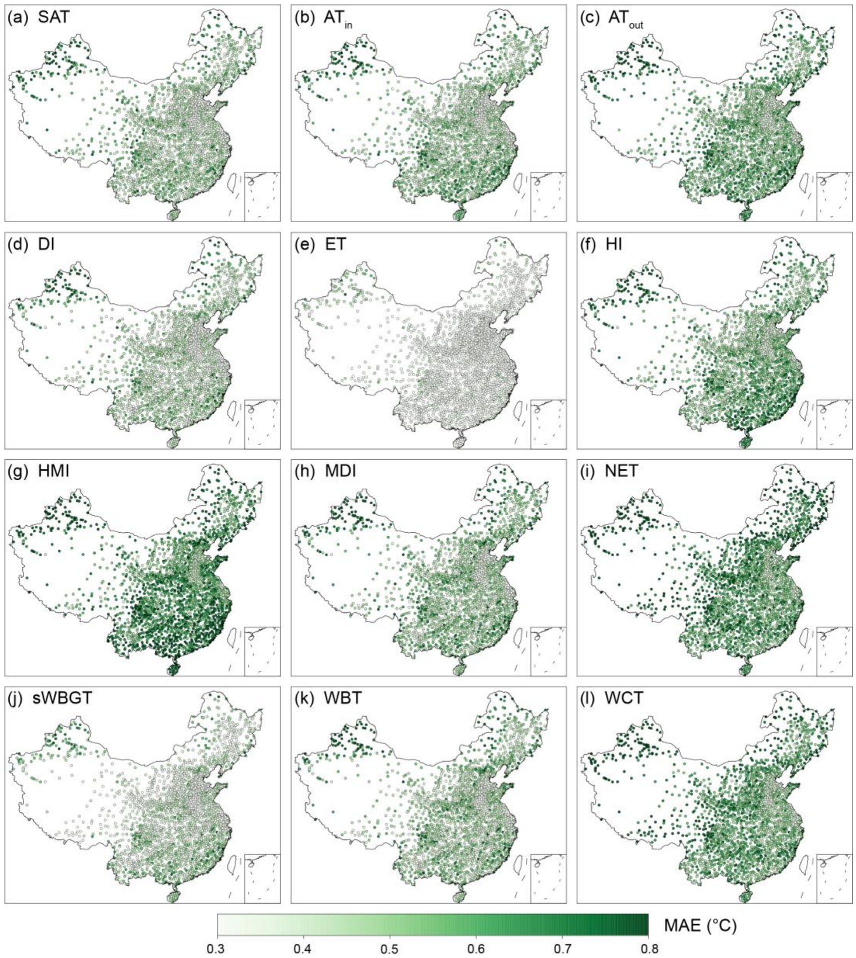

Figure 5. As Figure 4 but for *MAE*.

https://doi.org/10.5194/essd-2022-257
Preprint. Discussion started: 11 August 2022

Open Access Earth System Science Data Discussions

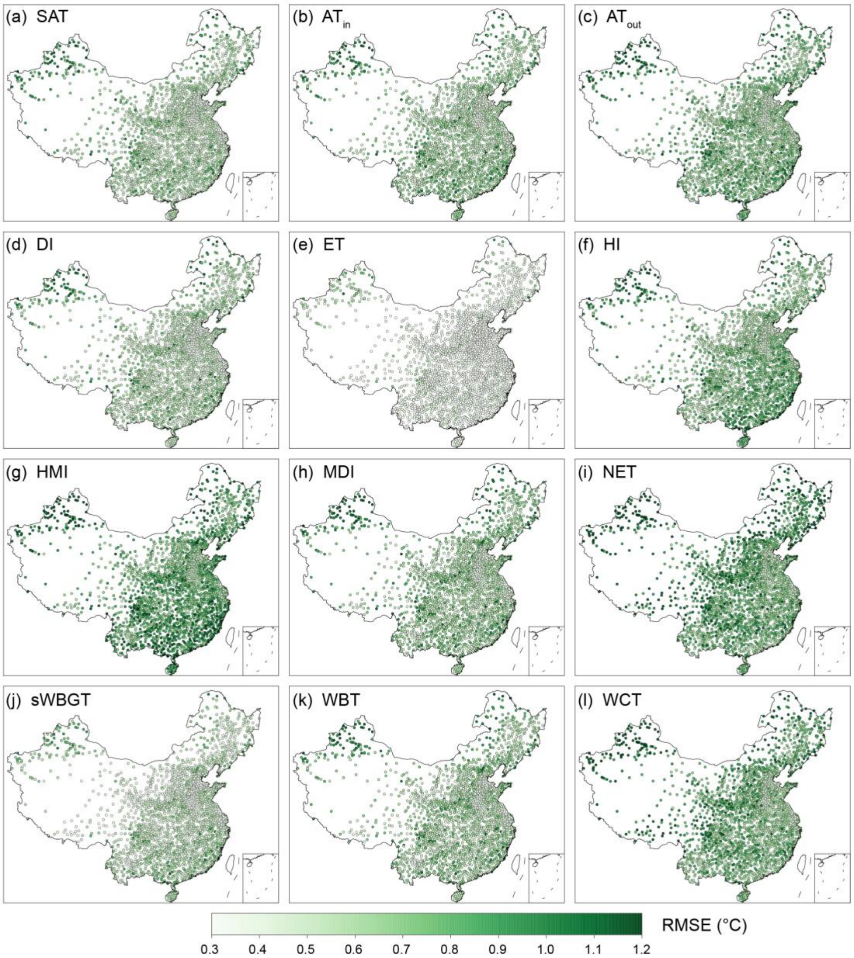

Figure 6. As Figure 4 but for *RMSE*.

https://doi.org/10.5194/essd-2022-257
Preprint. Discussion started: 11 August 2022

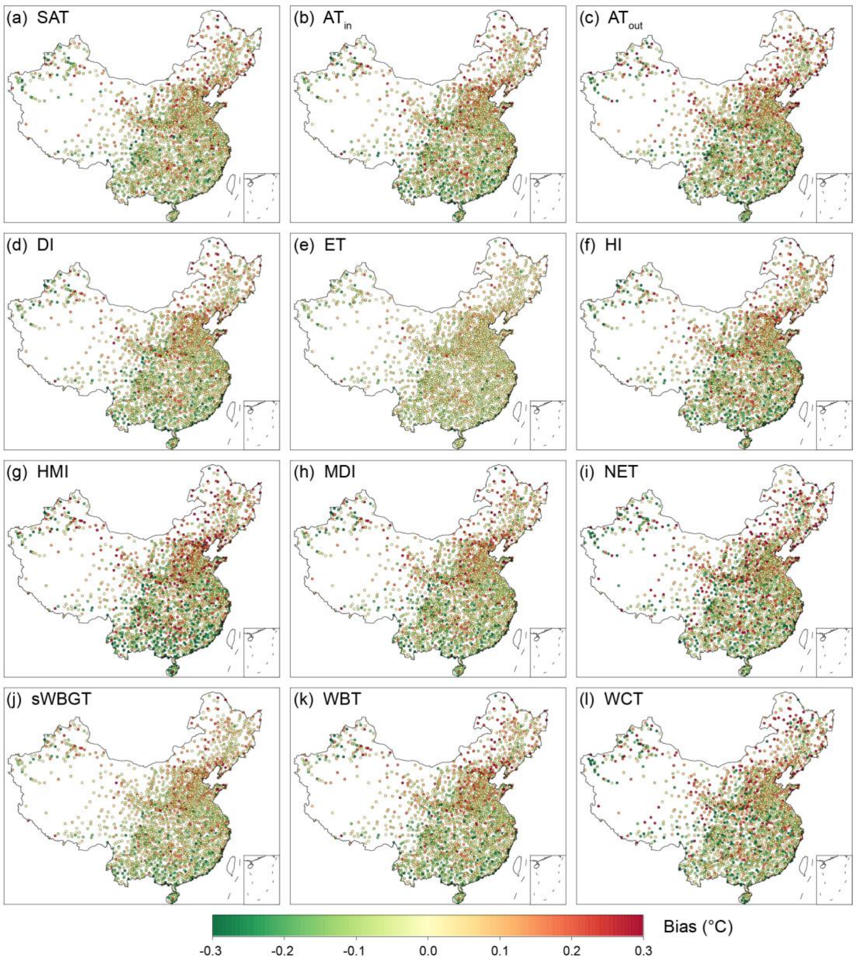

770 **Figure 7. As Figure 4 but for *Bias*.**

https://doi.org/10.5194/essd-2022-257
Preprint. Discussion started: 11 August 2022

Open Access Earth System Science Data Discussions

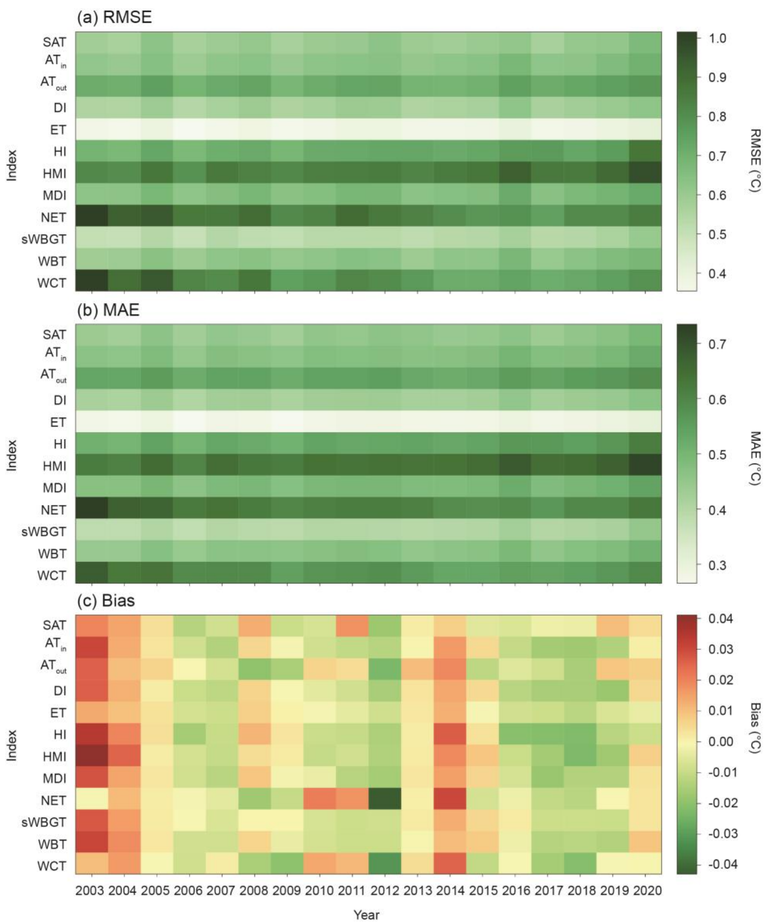

Figure 8. Prediction accuracies of human thermal indices in individual years over mainland China during 2003~2020.

https://doi.org/10.5194/essd-2022-257
Preprint. Discussion started: 11 August 2022

Open Access Earth System Science Data Discussions

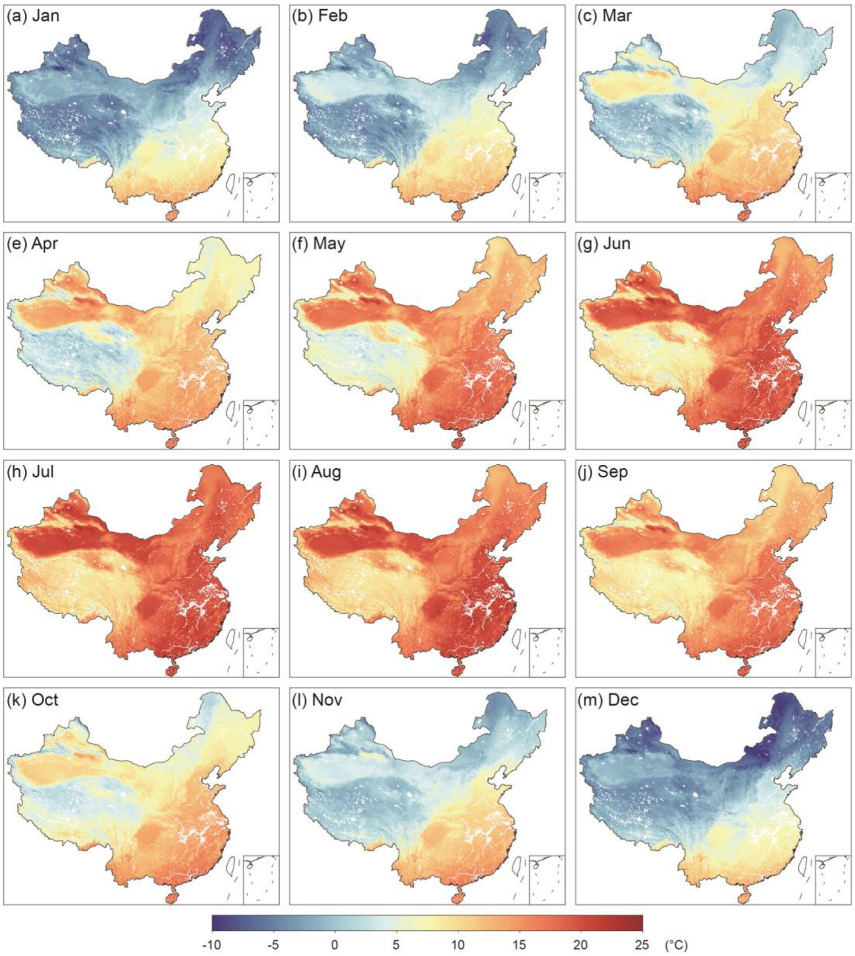

775 **Figure 9. Spatial distributions of monthly mean ET over mainland China in 2020.**

https://doi.org/10.5194/essd-2022-257
Preprint. Discussion started: 11 August 2022

Open Access Earth System Science Data Discussions

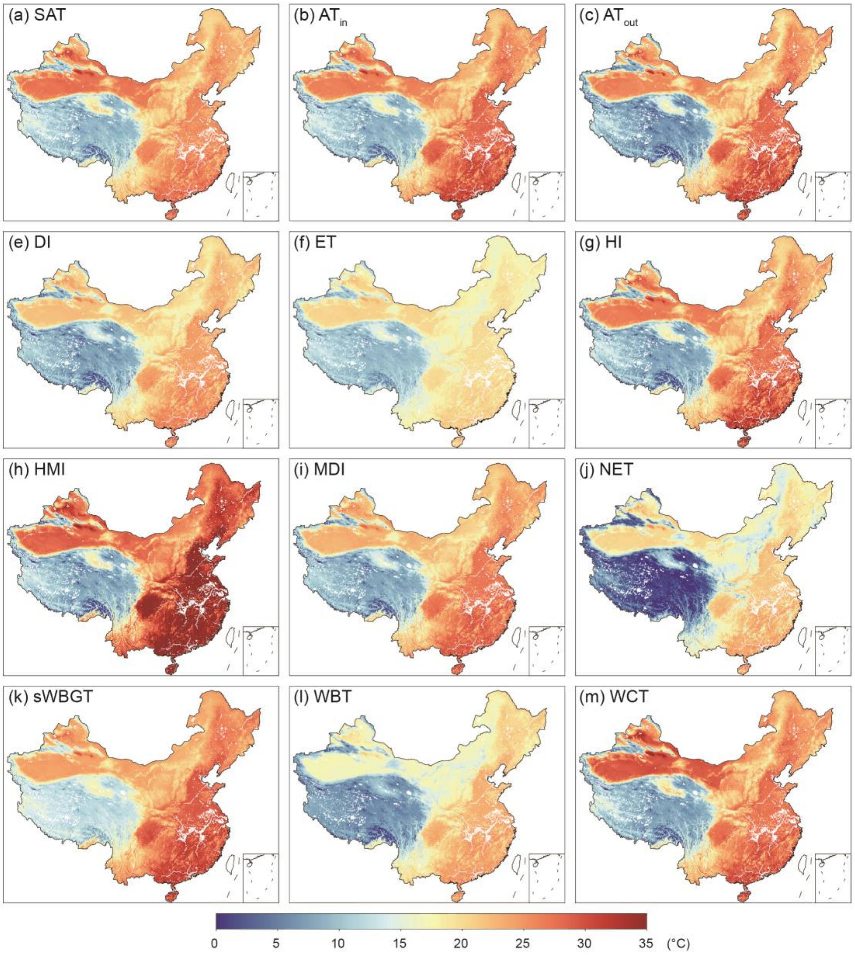

Figure 10. Spatial distributions of human thermal indices over mainland China in July 2020.

https://doi.org/10.5194/essd-2022-257
Preprint. Discussion started: 11 August 2022

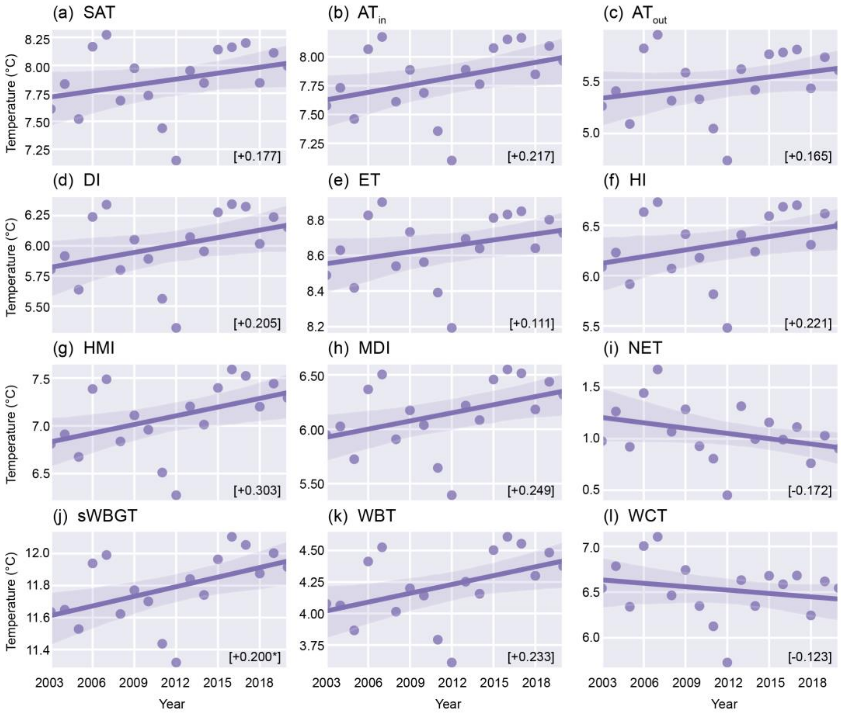

780 **Figure 11. Temporal variations of the national average of annual mean human thermal indices over mainland China during 2003~2020. The straight line illustrates the linear trend, the number in square bracket means the corresponding trend per decade, and the asterisk next to the number indicates that the trends are significant at the 0.05 level.**

https://doi.org/10.5194/essd-2022-257
Preprint. Discussion started: 11 August 2022

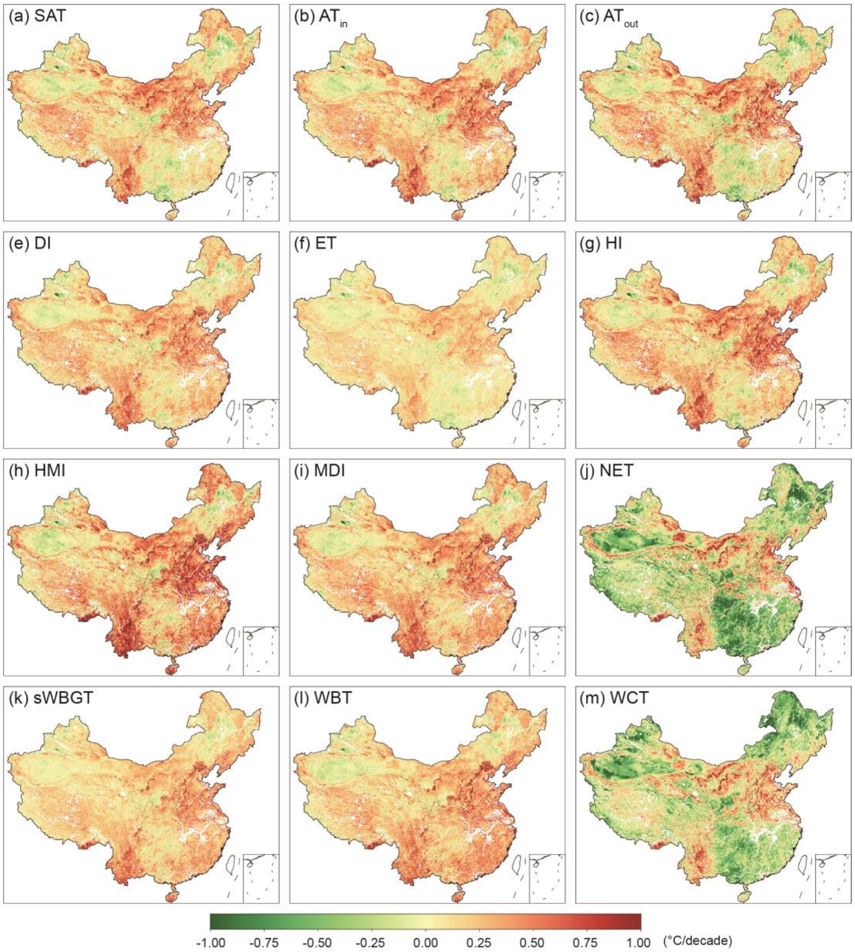

785 **Figure 12. Spatial distributions of the trends (unit: °C per decade) of annual mean human thermal indices over mainland China during 2003~2020.**

https://doi.org/10.5194/essd-2022-257
Preprint. Discussion started: 11 August 2022

Open Access Earth System Science Data Discussions

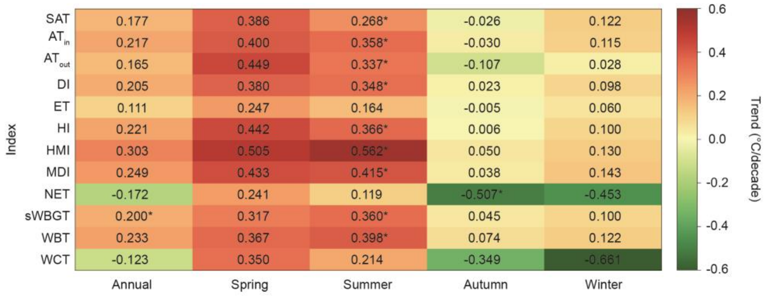

Figure 13. Temporal trends of the national average of annual and seasonal mean human thermal indices over mainland China during 2003~2020. The number means linear trend per decade. The asterisk indicates that the trends are significant at the 0.05 level.

https://doi.org/10.5194/essd-2022-257
Preprint. Discussion started: 11 August 2022

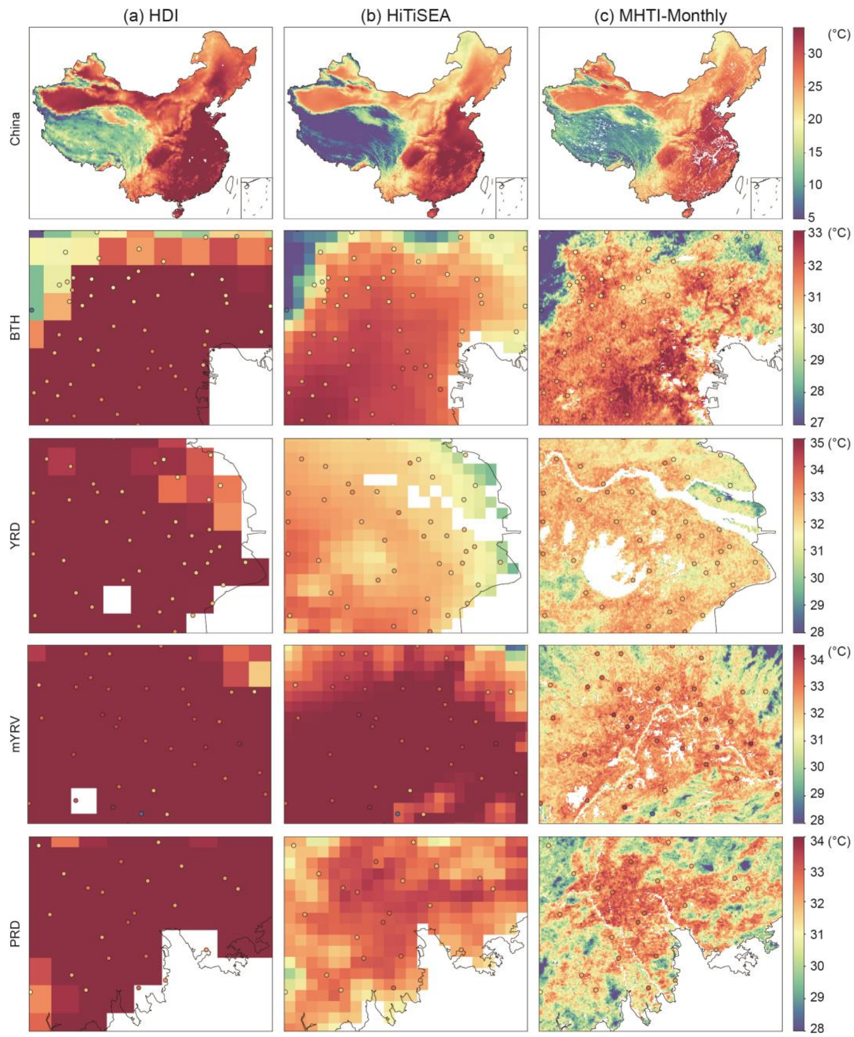

Figure 14. Comparison of the spatial patterns among HDI_0p25_1970_2018 (HDI), HiTiSEA, and HITIC-Monthly for AT_{in} in mainland China and four major UAs, i.e., Beijing-Tianjin-Hebei (BTH), Yangtze River Delta (YRD), middle Yangtze River Valley (mYRV) and Pearl River Delta (PRD), in July 2018. Colored circles indicate the observed AT_{in} values at individual meteorological stations.

Tables

Table 1. Grided datasets and variables used in this study.

Category	Dataset	Spatial Resolution	Temporal Resolution	Variables	Citation
Land surface temperature	A global seamless 1 km resolution daily land surface temperature dataset (2003-2020)	1 km×1 km	Daily	Land surface temperature	(Zhang et al., 2022b)
Land cover and land use	MCD12Q1.006	500 m×500 m	Annual	Main class of land cover and land use classes in 1 km×1 km pixels	(Sulla-Menashe and Friedl, 2019)
Elevation	MERIT DEM: Multi-Error-Removed Improved-Terrain DEM	90 m×90 m	/	Averaged Elevation in 1 km×1 km, averaged slope in 1 km×1 km pixels	(Yamazaki et al., 2017)
Impervious surface	Tsinghua/FROM-GLC/GAIA/v10	30 m×30 m	Annual	Proportion of impervious surface layer in 1 km×1 km pixels	(Gong et al., 2020)
Population density	WorldPop	1 km×1 km	Annual	Population density	(Gaughan et al., 2013)
Temporal variation	/	/	/	Year, Month	/

https://doi.org/10.5194/essd-2022-257
Preprint. Discussion started: 11 August 2022

Open Access Earth System Science Data Discussions

Table 2. Computation of human thermal indices.

Abbreviation	Human thermal index	Computation model	Reference
AT_{in}	Apparent Temperature (indoors)	$AT_{in} = -1.3 + 0.92 \times T + 2.2 \times E_a$	Steadman (1979)
AT_{out}	Apparent Temperature (outdoors, in the shade)	$AT_{out} = -2.7 + 1.04 \times T + 2 \times E_a - 0.65 \times V$	(Steadman, 1984)
DI	Discomfort Index	$DI = 0.5 \times WBT + 0.5 \times T$	(Sohar et al., 1963)
ET	Effective Temperature	$ET = T - 0.4 \times (T - 10) \times (1 - 0.001 * RH)$	(Gagge et al., 1972)
HI	Heat Index*	$HI^{*} = -8.784695 + 1.61139411 \times T - 2.338549 \times RH - 0.14611605 \times T \times RH - 1.2308094 \times 10^{-2} \times T^2 - 1.6424828 \times 10^{-2} \times RH^2 + 2.211732 \times 10^{-3} \times T^2 \times RH + 7.2546 \times 10^{-4} \times T \times RH^2 + 3.582 \times 10^{-6} \times T^2 \times RH^2$	(Rothfusz and Headquarters, 1990)
HMI	Humidex	$HMI = T + 0.5555 \times (0.1 \times E_a - 10)$	(Masterton et al., 1979)
MDI	Modified discomfort index	$MDI = 0.75 \times WBT + 0.38 \times T$	(Moran et al., 1998)
NET	Net Effective Temperature	$NET = 37 - \frac{37 - T}{0.68 - 0.0014 \times RH + \frac{1}{1.76 + 1.4 \times V^{0.75}}} - 0.29 \times T \times (1 - 0.01 \times RH)$	(Houghton and Yaglou, 1923)
sWBGT	simplified Wet Bulb Globe Temperature	$sWBGT = 0.567 \times T + 0.0393 \times E_a + 3.94$	(Gagge and Nishi, 1976)
WBT	Wet-bulb Temperature	$WBT = T \times atan(0.151977 \times (RH + 8.313659)^{0.5}) + atan(T + RH) - atan(RH - 1.676331) + 0.00391838 \times RH^{1.5} \times atan(0.02301 \times RH) - 4.686035$	(Stull, 2011)
WCT	Wind Chill Temperature	$WCT = 13.12 + 0.6215 \times T - 11.37 \times (V \times 3.6)^{0.16} + 0.3965 \times T \times (V \times 3.6)^{0.16}$	(Osczevski and Bluestein, 2005)

T is air temperature (°C), RH is relative humidity (%), V is wind speed (m/s), and E_a is actual water vapor pressure (kPa). Asterisk means that an adjustment is needed. All units of human thermal indices in this study are in degrees Celsius (°C).